Iron-induced skeletal muscle atrophy involves an Akt-forkhead box O3-E3 ubiquitin ligase-dependent pathway

Yasumasa Ikeda[1*], Mizuki Imao[2*], Akiho Satoh[2], Hiroaki Watanabe[3], Hirofumi Hamano[1,4], Yuya Horinouchi[1,4], Yuki Izawa-Ishizawa[1], Yoshitaka Kihira[1], Licht Miyamoto[2], Keisuke Ishizawa[3,4], Koichiro Tsuchiya[2], Toshiaki Tamaki[1]

[1]Department of Pharmacology, Institute of Biomedical Sciences, Tokushima University Graduate School, Tokushima, Japan

[2]Department of Medical Pharmacology, Institute of Biomedical Sciences, Tokushima University Graduate School, Tokushima, Japan

[3]Department of Clinical Pharmacy, Institute of Biomedical Sciences, Tokushima University Graduate School, Tokushima, Japan

[4]Department of Pharmacy, Tokushima University Hospital, Tokushima, Japan

* These authors equally contributed to this work.

Running title: Iron-induced atrophy via Akt-FOXO3-E3 Ubiquitin ligase pathway

Word count (excluding references and figure legends): 3542 words

Name and postal and email addresses for the corresponding author:

Yasumasa Ikeda

Associate Professor, Department of Pharmacology, Institute of Biomedical Sciences, Tokushima University Graduate School, Tokushima, 770-8503, Japan

E-mail: yasuike@tokushima-u.ac.jp

Phone: +81-88-633-7061; Fax: +81-88-633-7062

Abstract

Skeletal muscle wasting or sarcopenia is a critical health problem. Skeletal muscle atrophy is induced by an excess of iron, which is an essential trace metal for all living organisms. Excessive amounts of iron catalyze the formation of highly toxic hydroxyl radicals via the Fenton reaction. However, the molecular mechanism of iron-induced skeletal muscle atrophy has remained unclear. In this study, 8-weeks-old C57BL6/J mice were divided into 2 groups: vehicle-treated group and the iron-injected group (10 mg iron·day^{-1}·mouse^{-1}) during 2 weeks. Mice in the iron-injected group showed an increase in the iron content of the skeletal muscle and serum and ferritin levels in the muscle, along with reduced skeletal muscle mass. The skeletal muscle showed elevated mRNA expression of the muscle atrophy-related E3 ubiquitin ligases, atrogin-1 and muscle ring finger-1(MuRF1), on days 7 and 14 of iron treatment. Moreover, iron-treated mice showed reduced phosphorylation of Akt and forkhead box O3 (FOXO3a) in skeletal muscles. Inhibition of FOXO3a using siRNA *in vitro* in C2C12 myotube cells inhibited iron-induced upregulation of atrogin-1 and MuRF1 and reversed the reduction in myotube diameters. Iron-load caused oxidative stress, and an

oxidative stress inhibitor abrogated iron-induced muscle atrophy by reactivating the Akt-FOXO3 pathway. Iron-induced skeletal muscle atrophy is suggested to involve the E3 ubiquitin ligase mediated by the reduction of Akt-FOXO3a signaling by oxidative stress.

Keywords

iron, skeletal muscle atrophy, atrogenes

Introduction

Loss of skeletal muscle mass, also called muscle atrophy or sarcopenia, is induced by aging [1] and various chronic diseases such as heart failure [2], chronic kidney disease [3], diabetes [4] and other metabolic syndromes [5]. Muscle wasting debilitates quality of life and enhances the clinical outcome of morbidity or mortality [6]. Oxidative stress, which plays a crucial role in various pathological conditions, is also linked with diseased states of sarcopenia in disuse atrophy [7], chronic pulmonary obstruction [8], chronic kidney disease [9], sepsis [10] and heart failure [11]. Loss of muscle mass is induced by an imbalance between protein synthesis and degradation [12]. E3 Ubiquitin ligases such as atrogenes (Muscle Atrophy F-box (MAFbx)/atrogin-1 and Muscle RING Finger-1 [MuRF1]) are key regulators of protein degradation in the process of skeletal muscle atrophy [13,14].

Iron is an essential trace element for all living cells and organs. On the other hand, an excess of iron causes oxidative stress and catalysis of highly toxic hydroxyl-radicals via the Fenton reaction. Iron-mediated oxidative stress also causes various functional disorders via injury to DNA, lipids, enzymes, and proteins [2,15].

Free iron is toxic; thus it is detoxified and stored in intracellular ferritin [16]. Body iron storage, estimated by serum ferritin concentration, correlates with the excretion levels of an oxidative stress marker, urinary 8-hydroxy-2'-deoxyguanosine, regardless of age or gender [17]. Iron overload disorders (e.g. hereditary hemochromatosis or thalassemia) present various complications such as cardiomyopathy, liver cirrhosis, and diabetes due to ectopic iron accumulation [18]. Body iron content is also associated with the pathological conditions with no iron overload, such as liver diseases [19], obesity [20], diabetes [21,22], cardiovascular diseases [23,24], and kidney diseases [25]. In fact, clinical [26,27,28] and experimental studies [29,30,31,32] show that these diseases are suppressed by reducing body iron content. Thus, iron plays a crucial role in pathology of non-iron overload diseases, as well as hereditary iron overload diseases.

Several studies have shown the involvement of iron accumulation in sarcopenia with aging. In aged rats, skeletal muscle mass is reduced along with increased iron accumulation [33,34,35] due to changes in iron metabolism. In skeletal muscle of aged rats, iron regulatory protein 2 (IRP2) is downregulated, leading to the reduced expression of transferrin receptor-1 (an iron transporter) and the increased

expression of ferritin (an iron storage protein) [34]. Divalent metal transporter-1 and Zip14 (a member of the SLC39A zinc transporter family), which are involved in iron uptake into cells, are upregulated, and FPN expression is relatively low in skeletal muscles of aged rats [36]. These changes in iron metabolism are consistent with the accelerated accumulation of iron in skeletal muscles. Moreover, acute muscle atrophy induced by hindlimb suspension, a model of disuse atrophy, promotes further iron accumulation, and it is associated with extensive oxidative stress after reloading in skeletal muscles of aged rat [36]. Two clinical studies showed that ferritin levels are higher in sarcopenic obese people [37] or in women with sarcopenia [38]. In addition, iron administration induces sarcopenia and oxidative stress in skeletal muscles of mice [39]. Thus, a strong association of iron accumulation with skeletal muscle atrophy is suggested. However, the precise molecular mechanism of iron-induced muscle atrophy remains to be elucidated.

In the present study, we found that iron administration upregulated atrogin-1 and MuRF1 expression concomitantly with skeletal muscle atrophy and induction of oxidative stress. The induction of atrogenes by iron loading was involved in the

suppression of Akt-forkhead box O3 (FOXO3a) signaling pathway via excess iron-mediated oxidative stress.

Materials and Methods

Chemicals and reagents

The following commercially available antibodies were used for this study: anti-phospho-FKHRL1 (FOXO3a) (Ser253) antibody (Santa Cruz Biotechnology, Santa Cruz, CA, USA); anti-phospho Akt (Ser473) antibody, anti-total Akt antibody, and anti-FOXO3a antibody (Cell Signaling Technology, Danvers, MA, USA); anti-ferritin heavy chain antibody and anti-ferritin light chain (Santa Cruz Biotechnology); and anti-tubulin antibody as a loading control (Calbiochem, San Diego, CA, USA). Tempol (4-Hydroxy-TEMPO) was purchased from Sigma-Aldrich Inc. (Tokyo, Japan).

Experimental animals and treatment

All experimental procedures involving animals were implemented in accordance with the guidelines of the Animal Research Committee of Tokushima University Graduate School, and with approval from the Tokushima University Institutional Review Board for animal protection. Male C57BL/6J mice were purchased from CLEA Japan Inc.

(Tokyo, Japan). Eight-week-old mice used for the study were maintained in a room under conventional conditions with a regular 12-h light/dark cycle and fed with free access to food (Type NMF, 10 mg Fe/100 g food; Oriental Yeast, Tokyo, Japan) during the study. The mice were intraperitoneally injected with iron-dextran once daily (10 mg iron-dextran/single-dose: 200 μl) or an equal volume of vehicle [39]. At 24 h after the last injection of iron-dextran, mice were sacrificed by an over-dose of pentobarbital and were used for analysis on days 1, 3, 7, and 14.

Measurement of serum ferritin levels

Serum ferritin concentration was determined with a Mouse Ferritin enzyme-linked immunosorbent assay (ELISA) kit (Immunology Consultants Laboratory, Newberg, OR, USA). Serum diluted by 20% was used for the assay [29].

Measurement of iron concentrations in skeletal muscles

Iron concentrations in skeletal muscle were measured using the Metallo assay kit as previously described (Metallogenics Co., Ltd., Chiba, Japan) [32,40]. In brief, the extracted muscle (approximately 50 mg muscle per piece) was weighed and mechanically homogenized in 500 μl lysis buffer (T-PER Tissue Protein Extraction

Reagent, Thermo Fischer Scientific Inc., Waltham, MA USA) with protease inhibitor (cOmplete™, Mini, EDTA-free, Roche Diagnostics K.K., Tokyo, Japan) and phosphatase inhibitor (PhosSTOP Phosphatase Inhibitor Cocktail (Roche Diagnostics K.K.). The crude lysates were further lysed with an ultrasonic sonicator, HCL was added (0.01 M final concentration), and the mixture was incubated for 30 min with mixing at every 10 min. The lysate was centrifuged at 4°C for 15 min, and the supernatant was used to assay iron concentration. Tissue iron concentration was normalized to tissue wet weight and expressed as $\mu g \cdot g^{-1}$ tissue.

Histological analysis

After sacrifice, the skeletal muscle of mice was excised following normal saline perfusion. A gastrocnemius muscle was fixed overnight in 4% paraformaldehyde at 4°C and embedded in paraffin. Sections of 3-μm thickness were prepared and stained with hematoxylin-eosin to measure muscle fiber area. Area measurements of at least 100 fibers were obtained for each animal from 10 randomly selected fields in 5 different sections. Muscle area was quantified using ImageJ 1.38x software (National Institutes of Health, Bethesda, MD).

Quantitative measurement of mRNA expression levels

Total RNA extraction, cDNA synthesis, and quantitative real-time RT-PCR were performed as described previously [32]. In brief, total RNA was extracted with RNAiso reagent (Takara Bio, Inc., Otsu, Japan), and cDNA was synthesized using the PrimeScript® RT Reagent Kit with gDNA Eraser (Takara Bio) according to the manufacturer's instructions. Quantitative real-time RT-PCR was performed using the iCycler MyiQ2 Real-Time PCR Detection System (Bio-Rad Laboratories Inc., Hercules, CA, USA) with SYBR Green reagent (Thunderbird SYBR qPCR Mix, Toyobo Co., Ltd., Osaka, Japan). The primer sets used were as follows: 5′-AGCGCTTCTTGGATGAGAAA-3′ and 5′-GGCTGCTGAACAGATTCTCC-3′ for mouse *MAFbx/atrogin-1*, 5′-GAGCAGCTGGAAAAGTCCAC-3′ and 5′-CTTGGCACTTGAGAGGAAGG-3′ for mouse *muscle ting finger-1 (MuRF1)*, and 5′-GCTCCAAGCAGATGCAGCA-3′ and 5′-CCGGATGTGAGGCAGCAG-3′ for *36B4* as an internal control. The expression levels of all target genes were normalized using *36B4*, and the values were expressed as relative fold change compared to the values of the control group (set to 1.0).

Western blotting

Protein expression and phosphorylation levels were evaluated by western blotting. The method of protein extraction and sample preparation from tissues and cells has been described previously [32]. In brief, cells and tissues were homogenized and sonicated in lysis buffer with protease and phosphatase inhibitors and for protein extraction. The samples were boiled for 5 min in Laemmli sample buffer, separated using SDS-PAGE and transferred onto a polyvinylidene difluoride membrane. A chemiluminescence reagent was used for detection of immunoreactive bands. Immunoblot bands were visualized by exposure onto X-ray film or by C-DiGit chemiluminescent scanner (LI-COR C-DiGit Blot Scanner, Lincoln, Nebraska, USA). Semi-quantitative analysis of immunoblotting was performed by densitometry using ImageJ 1.38x software (U. S. National Institutes of Health, Bethesda, Maryland, USA, http://imagej.nih.gov/ij/, 1997-2014). The levels of phosphorylated Akt and FOXO3a were normalized to total Akt and FOXO3a, respectively. The protein levels of ferritin were normalized with tubulin. The amount of protein loaded was also checked by both detection of tubulin bands and staining for all protein bands in the membrane (MemCode Reversible Protein

Stain kit; Thermo Fisher Scientific Inc., Waltham, MA). The antibodies were used at the following dilutions: anti-phospho Akt (1:500), anti-total Akt (1:1000), anti-phospho-FOXO3a (1:250), anti-total FOXO3a (1:1000), ferritin heavy chain (1:250), ferritin light chain (1:250), and anti-tubulin (1:1000).

Cell culture

C2C12 myoblast cells were purchased from DS Pharma Biomedical Co., Ltd. (Osaka, Japan) and were maintained and sub-cultured in DMEM containing 10% FBS, according to the culture protocol. The cells were used up to the 5th-7th passages. The cells were grown to sub-confluence for about 24-48 h, and the media was replaced with DMEM containing 2% horse serum, and incubated for 4 days to stimulate myotube formation. We used iron sulfate ($FeSO_4$) for *in vitro* studies. Iron sulfate was dissolved in water and added to cell culture media. Differentiated C2C12 myotube cells were treated with 100 μM iron sulfate for indicated durations.

In situ tissue superoxide detection.

Superoxide production of skeletal muscle or myotubes was evaluated by dihydroethidium (DHE) staining method as described previously [32]. In brief, frozen

tissue sections or non-fixed cells were incubated with DHE in PBS (10 μM) in a dark, humidified container at room temperature for 30 min and then observed using fluorescence microscopy.

Small interfering RNA (siRNA) experiments

siRNA targeting mouse FOXO3a and a non-targeting siRNA control sequence were purchased from Cell Signaling Technology. Transfection was performed as described previously [40]. Briefly, the differentiation induced C2C12 cells after 2 days were transfected with 50 nM siRNA using RNAiMAX® reagent and OPTI-MEM® (Life Technologies, Inc.). Cells were used for further experiments after 48 h of transfection (4 days later after starting differentiation).

Measurement of myotube size

Myotube size was quantified by measuring diameter of 100 myotubes from 10 random fields at 100× magnification using Image J software. On an average, 5 diameter measurements were taken along the length of the myotube and the mean diameter was calculated. The values were expressed as relative fold change compared to the values of the control group (set to 100).

Statistical analysis

Data are expressed as mean ± standard error of the mean (SEM). An unpaired two-tailed Student's *t*-test was used for comparison between two groups. For comparison among multiple groups, statistical significance was analyzed using two-way ANOVA, and the significance of each difference was determined by post-hoc testing using Dunnett's method or Tukey–Kramer method. The results were considered significant at $P < 0.05$.

Results

Iron-induced skeletal muscle atrophy in mice

We evaluated the effect of iron treatment on body weight, skeletal muscle weight, and iron levels. As shown in Table 1, there were no differences in body weight between vehicle-treated group and the iron-treated group on day 7 and 14. The weights of gastrocnemius, soleus, and tibialis anterior muscles were significantly lower in the iron-treated group than in the vehicle-treated group on days 7 and 14. Histological analysis of representative images showed that mean size and muscle fiber area of gastrocnemius muscles was lower in iron-treated mice compared to vehicle-treated mice on day 7 and 14. The distribution of muscle fiber size showed that iron administration

increased the proportion of small-sized muscle fibers and reduced the proportion of large-sized muscle fibers (Figure 1A).

Skeletal muscle iron concentration was increased by whole body iron load

In terms of iron status, muscle iron concentration and serum ferritin levels were significantly higher in iron-treated mice at days 3, 7, and 14 (Table 2). The protein expressions of ferritin heavy chain and ferritin light chain, iron storage proteins, were significantly elevated at day 3, 7 and 14 in skeletal muscles of iron-treated mice (Figure 1F).

Iron treatment induced mRNA expression of E3 ubiquitin ligase, atrogin-1 and MuRF1 in skeletal muscle of mice

E3 Ubiquitin ligases, including atrogin-1 and MuRF1, are key regulators of skeletal muscle atrophy [13,14]. Therefore, we examined their involvement in iron-induced skeletal muscle atrophy and observed that iron loading augmented the mRNA expression of atrogin-1 and MuRF1 in murine skeletal muscles at day 7 and later (Figure 2A).

Effects of iron load on Akt-FOXO3 pathway in skeletal muscle

Akt-FOXO3 signaling is critical in regulating the expression of E3 ubiquitin ligases [41,42]. Therefore, we checked the involvement of Akt-FOXO3 signaling in iron-induced expression of atrogin-1 and MuRF1. Iron treatment decreased FOXO3a phosphorylation on days 3, 7 and 14. Similarly, Akt phosphorylation was also reduced on day 3, 7 and 14 (Figure 2B).

Effects of iron on E3 ubiquitin ligase expression and Akt-FOXO3a signaling in an in vitro study

We also examined the effects of iron on E3 ubiquitin ligase expression and Akt-FOXO3a signaling *in vitro* using differentiated C2C12 myotube cells. Iron treatment increased the expression of atrogin-1 and MuRF1 at 8 h (Figure 3A). The levels of phosphorylated Akt and FOXO3 were decreased at 60 min after iron stimulation (Figure 3B). Morphological analysis showed myotube atrophy at 48 h after iron treatment (Figure 3C).

Involvement of FOXO3a in Iron-induced myotube atrophy via E3 ubiquitin ligase

To determine whether iron upregulates E3 ubiquitin ligase expression through a FOXO3a-dependent pathway, we silenced FOXO3a using siRNA. Transfection with

FOXO3a siRNA resulted in approximately 50% reduction of FOXO3a mRNA and protein levels as compared to the control siRNA-transfected cells (Figure 4A). FOXO3a silencing suppressed iron-induced atrogin-1 and MuRF1 expression (Figure 4B) and prevented iron-induced myotube atrophy in C2C12 cells (Figure 4C).

Involvement of iron-mediated oxidative stress in the Akt-FOXO3-E3 ubiquitin ligase pathway in muscle atrophy

An excess iron causes oxidative stress. In the present study, iron-treated mice showed increased superoxide production in the skeletal muscles (Figure 1D and E). Similarly, iron also induced superoxide production in C2C12 myotubes (Figure 3D). To determine the involvement of iron-mediated oxidative stress in skeletal muscle atrophy, we used a radical scavenger reagent, Tempol. As shown in Figure 5A, Tempol suppressed upregulation of iron-induced E3 ubiquitin ligase in C2C12 myotube cells. Tempol pre-treatment also prevented iron-induced reduction of Akt and FOXO3a phosphorylation (Figure 5B). Additionally, Tempol treatment inhibited iron-induced myotube atrophy (Figure 5C).

Discussion

In the present study, an excess of iron induced skeletal muscle atrophy and augmented oxidative stress. Iron loading stimulated mRNA expression of the E3 ubiquitin ligases, atrogin-1 and MuRF1, and decreased the phosphorylation of Akt and FOXO3a, which resulted in decreased skeletal muscle mass. In correspondence with the in vivo model, iron treatment induced myotube atrophy, expression of E3 ubiquitin-ligases, and reduced phosphorylation of Akt and FOXO3a in an *in vitro* system as well. The iron-induced myotube atrophy and upregulation of E3 ubiquitin-ligases were inhibited by FOXO3a silencing and Tempol treatment. These findings indicated that iron induced skeletal muscle atrophy through Akt-FOXO3a-atrogenes (atrogin-1 and MuRF1) pathway by producing oxidative stress.

Iron-mediated oxidative stress is thought to be involved in the pathology of hereditary iron overload diseases as well as non-hereditary diseases such as hepatitis C [19], obesity [20], diabetes [21,22] and cardio-renal vascular diseases [23,24,25]. Generally, body iron content is estimated by serum ferritin and it is elevated in the above diseases. Ferritin synthase is mainly regulated by iron at the translational level through iron-regulatory protein and iron-responsive elements in the 5′-untranslated

regions of ferritin mRNA [43]. Serum ferritin reflects stored body iron and is a useful indicator of body iron content [44], although the original source and the secretion mechanism of serum ferritin are not completely understood. On the other hand, ferritin is an acute-phase reactant protein that is synthesized upon induction by inflammatory cytokines such as TNF-α [45], IL-1ß, and IL-6 [46]. Chronic inflammation is widely recognized as a major pathogenic mechanism and is associated with obesity and metabolic diseases including diabetes and cardiovascular diseases [47,48]. Therefore, increased serum ferritin levels might be caused by not only increased iron content but also by inflammatory processes in certain clinical diseases. Nevertheless, serum ferritin levels have been used as a unique marker of body iron content.

It is normally recognized that body iron content (evaluated by serum ferritin) or oxidative stress increases and skeletal muscle mass decreases with aging in humans. Several animal studies have reported that iron accumulation is also associated with atrophic change and oxidative stress in the skeletal muscles. Aged rats showed skeletal muscle atrophy, increased iron amount and oxidative stress in the skeletal muscle compared to young rats [35,36] In suspension-induced atrophied hindlimb muscles,

muscle mass negatively correlates with RNA oxidative damage and iron content in skeletal muscles of either aging or disuse [49]. Deferoxamine, an iron chelator, alleviates immobilization-induced skeletal muscle atrophy by reducing oxidative stress [50]. Iron-treated mice present with increased oxidative stress in muscles along with reduced exercise performance [39]. In agreement with the above studies, we demonstrated that mice treated with excessive iron treatment demonstrated skeletal muscle atrophy and increased oxidative stress. Thus, iron accumulation is suggested to be directly associated with skeletal muscle atrophy via increased oxidative stress. In terms of iron metabolism in atrophied muscle, IRP2 is an important regulator of muscle iron amount via regulation of TfR1 and ferritin expression in aged rats [34]. Increased expression of iron importers (DMT-1 and Zip14) and relative low expression of FPN are seen in muscle of either age or disuse, resulting in an ineffective iron export upon iron overload [36]. Taken together, the change of iron metabolism might be involved in consequent iron accumulation, contributing to a vicious cycle formation of further muscle atrophy through oxidative stress. However, the change of iron metabolism in the process of muscle atrophy with age and disuse remains unclear. Further studies are necessary to

elucidate the relationship between iron metabolism and the process of skeletal muscle atrophy.

Increased protein degradation is one of the mechanisms of skeletal muscle atrophy, suggesting the importance of the balance between anabolic and catabolic processes [12,51]. In the catabolic process, E3 Ubiquitin ligases are involved in the selection of substrates for ubiquitination and subsequent proteasomal degradation [52,53]. Two studies in 2001 demonstrated that the E3 Ubiquitin ligases, atrogin-1 and MuRF1, play key regulatory roles in protein degradation during muscle atrophy [13,14]. Atrogin-1 and MuRF1 are upregulated under a multitude conditions inducing muscle atrophy including immobilization, hindlimb unloading, dexamethasone, starvation and cachexia [14,53,54]. Indeed, the mice with genetically ablated atrogin-1 and MuRF1 were shown to preserve muscle mass [13,14]. Therefore, these genes are thought to be typical markers for the process of muscle atrophy. In the present study, an excess iron loading increased the expression of atrogin-1 and MuRF1 in the skeletal muscle consequently leading to muscle atrophy, thus indicating the involvement of E3 ubiquitin ligases in iron-induced skeletal muscle atrophy.

The E3 Ubiquitin ligases, atrogin-1 and MuRF1, are transcriptionally regulated by the class O-type forkhead transcriptional factors (FOXOs). Constitutively activate FOXO3a enhanced atrogin-1 promoter and induced skeletal muscle atrophy [55]. Activation of FOXO3 is necessary for atrophic induction through upregulation of atrogin-1 and MuRF1 [56,57]. On the other hand, increased expression of MuRF1 as well as atrogin-1, was necessary but not sufficient for FOXO1 activation [41], and FOXO1 transgenic mice showed skeletal muscle atrophy [58,59]. In the present study, iron inhibited FOXO3 phosphorylation in skeletal muscle of mice and in C2C12 myotube cells. Moreover, FOXO3 silencing prevented iron-induced atrogin-1 and MuRF1 upregulation. These findings suggest that iron-induced atrogin-1 and MuRF1 expression are involved in FOXO3 transcriptional regulation.

Akt activation is involved in multiple signaling pathways including the process of skeletal muscle atrophy through the transcriptional regulation of atrogin-1 and MuRF1 via inhibiting FOXOs translocation into nucleus [41,42]. Therefore, the Akt-FOXO pathway plays a crucial role in the transcriptional regulation of E3 ubiquitin ligases during skeletal muscle atrophy. In the present study, we demonstrated that

excessive iron induced oxidative stress and Akt inactivation in the skeletal muscle. In an *in vitro* experiment, Tempol, an anti-oxidant drug, ameliorated iron-induced skeletal muscle atrophy by inhibiting the upregulation of atrogin-1 and MuRF1 and restoration of Akt-FOXO3a inactivation. Indeed, an excess of iron causes cardiac damage through apoptosis induction via Akt inactivation, and is reversed by iron chelator administration [60]. Moreover, iron restriction is shown to ameliorate Akt inactivation, as well as increased oxidative stress in cardiovascular tissues [30]. Therefore, iron-induced oxidative stress is suggested to suppress Akt activation, consequent to the promotion of nuclear translocation of FOXO3 and transcriptional activation of E3 ubiquitin ligase in skeletal muscles.

In conclusion, excessive iron induces skeletal muscle wasting through Akt-FOXO3-dependent E3 ubiquitin ligase activation and oxidative stress. These findings suggest a new mechanism of sarcopenia due to iron accumulation and indicate the modulation of iron as a potent therapeutic target for skeletal muscle atrophy.

Funding

This work was supported by JAPAN FOUNDATION FOR AGING and HEALTH Research Grant, Mitsui Sumitomo Insurance Welfare Foundation Research Grant, The Nakatomi Foundation, and JSPS KAKENHI Grant (No. 15K01716) to Y.I.

Author contributions

1. Conception or design of the work; YI

2. Acquisition, analysis, or interpretation of data for the work; YI, MI, AS, HW, HH, YH, YI-I, YK, LM, KI, KT, TT

3. Drafting the work or revising it critically for important intellectual content: YI, MI, TT

Acknowledgement

We thank Editage (www.editage.jp) for English language editing.

Conflict of interest

There is no conflict of interest in this article.

FIGURE LEGENDS

Figure 1. Excess iron-induced skeletal muscle atrophy in mice. (A) Left panel:

Representative images of gastrocnemius muscles from mice at day 7 and 14 after vehicle or iron treatment. (B) The average size of myofiber areas from mice at day 7 and 14 after vehicle or iron treatment. Results are expressed as mean ± standard error of mean (SEM). $^{**}P < 0.01$ vs. vehicle treatment. (C) The distribution of myofiber sizes in gastrocnemius muscles from vehicle or iron-treated mice. Values are expressed as means ± SEM. $n = 4$ in each group. (D) Representative images of DHE staining of skeletal muscle. (E) Quantitative analysis of relative fluorescence intensity. Relative fold change is normalized to value of the vehicle group (set to 1.0). Values are expressed as means ± SEM, $n = 4$–5 in each group. $^{*}P < 0.05$ vs. vehicle treatment. (F) Effects of iron treatment on ferritin expression in skeletal muscles. Semi-quantitative analysis of densitometry for ferritin heavy chain and ferritin light chain normalized to tubulin. Relative fold change is normalized to value of the vehicle group (set to 1.0). Values are expressed as means ± SEM. $^{*}P < 0.05$, $^{**}P < 0.01$ vs. vehicle-treated mice. $n = 12$ in each group.

Figure 2. (A) Changes in mRNA expression of E3 ubiquitin ligase genes from skeletal

muscles of vehicle- or iron-treated mice. Quantitative real-time reverse transcriptase-polymerase chain reaction (RT-PCR) analysis of atrogin-1 and MuRF1. Relative fold change is normalized to value of the vehicle group (set to 1.0). Values are expressed as means ± SEM. *$P < 0.05$, **$P < 0.01$ vs. vehicle treated mice. $n = 4$–8 in each group. (B) Effects of iron treatment on Akt and FOXO3a activation. Semi-quantitative analysis of densitometry for phospho-Akt and phospho-FOXO3a normalized by total-Akt and total FOXO3a, respectively. Relative fold change is normalized to value of the vehicle group (set to 1.0). Values are expressed as means ± SEM. *$P < 0.05$, **$P < 0.01$ vs. vehicle-treated mice. $n = 8$ in each group.

Figure 3. Effect of iron stimulation on myofiber atrophy in C2C12 myotube cells. (A) Left panel: The time course changes of atrogin-1 mRNA expression after iron-treatment in C2C12 myotube cells. Relative fold change is normalized to value of the control group (at time 0) (set to 1.0). Values are expressed as means ± SEM. **$P < 0.01$ vs. vehicle treatment at the same time. $n = 4$–8 in each group. Right panel: mRNA expression of atrogin-1 and MuRF1 at 8 h after vehicle or $FeSO_4$ stimulation. Relative

fold change is normalized to value of the control group (set to 1.0). Values are expressed as means ± SEM. $^{**}P < 0.01$. $n = 8$ in each group. (B) Left panel: Representative figures of time-course changes of Akt- and FOXO3a-phosphorylation and protein expression after iron treatment in C2C12 myotube cells. Right panel: Semi-quantitative analysis of densitometry for Akt and FOXO3a phosphorylation normalized by total-Akt and FOXO3a, respectively. Relative fold change is normalized to value of the control group (at time 0) (set to 1.0). Values are expressed as means ± SEM. $^{*}P < 0.05$, $^{**}P < 0.01$ vs. 0 min. $n = 8$ in each group. (C) Left panel: Representative morphology of myotubes at 48 h after vehicle or $FeSO_4$ treatment. Right panel: Quantitative analysis of myotube diameter. Relative fold change is normalized to value of the control group (set to 100). Values are expressed as means ± SEM. $^{*}P < 0.05$, $^{**}P < 0.01$. $n = 4$ in each group. (D) Left panel: Representative images of DHE staining of myotube cells after 30 min with or without $FeSO_4$ stimulation. Right Panel: Quantitative analysis of relative fluorescence intensity. Relative fold change is normalized to value of the control group (set to 1.0). Values are expressed as means ± SEM, $n = 9$ in each group. $^{*}P < 0.05$ vs. vehicle treatment.

Figure 4. The involvement of FOXO3a in iron-induced myofiber atrophy.

(A) C2C12 myotube cells were transfected with 50 nM FOXO3a siRNA. FOXO3a expression levels of mRNA (level panel) and protein (right panel) were reduced after treatment with FOXO3a siRNA. Relative fold change is normalized to value of the unrelated siRNA group (set to 1.0). Values are expressed as means ± SEM. *$P < 0.05$, n = 4 in each group. (B) Treatment with FOXO3a siRNA inhibited iron-induced atrogin-1 and MuRF1 upregulation in C2C12 myotube cells. Forty-eight h after siRNA transfection, cells were treated with 100 μM $FeSO_4$ or vehicle for 8 h, Relative fold change is normalized to value of the unrelated siRNA group (set to 1.0). Values are expressed as means ± SEM. *$P < 0.05$, **$P < 0.01$. n = 8–12 in each group. (C) Left panel: Representative morphology of myofibers at 48 h after vehicle or iron treatment with unrelated siRNA or FOXO3a siRNA transfection. Right panel: Quantitative analysis of myotube diameter. Relative fold change is normalized to value of the unrelated siRNA group (set to 100). Values are expressed as means ± SEM. *$P < 0.05$, **$P < 0.01$. $n = 8$ in each group.

Figure 5. The involvement of iron-induced muscle atrophy mediated by Akt-FOXO3-E3 ubiquitin ligase pathway via oxidative stress

(A) Pretreatment with Tempol inhibited iron-induced atrogin-1 and MuRF1 upregulation in C2C12 myotube cells. Differentiated cells were treated with 100 μM $FeSO_4$ or vehicle for 8 h after pretreatment with vehicle or 100 μM Tempol. Relative fold change is normalized to value of the control group (set to 1.0). Values are expressed as means ± SEM. $*P < 0.05$, $**P < 0.01$. n = 8 in each group. (B) Left panel: Representative figures of Akt- and FOXO3a-phosphorylation and protein expression after iron treatment in C2C12 myotube cells. Right panel: Semi-quantitative analysis of densitometry for phospho-Akt, and phospho-FOXO3a corrected by total-Akt and FOXO3a, respectively. Relative fold change is normalized to value of the control group (Fe+Vehicle treatment at time 0)(set to 1.0). Values are expressed as means ± SEM. $*P < 0.05$, $**P < 0.01$. Values are expressed as means ± SEM. $*P < 0.05$, $**P < 0.01$. $n = 8$ in each group. (C) Left panel: Representative morphology of myofibers at 48 h after vehicle or $FeSO_4$ treatment with or without Tempol. Right panel: Quantitative analysis

of myotube diameter. Relative fold change is normalized to value of the control group (set to 100). Values are expressed as means ± SEM. *$P < 0.05$, **$P < 0.01$. The values are expressed as means ± SEM. *$P < 0.05$, **$P < 0.01$. $n = 6$ in each group.

References

[1] W.J. Evans, What is sarcopenia?, J Gerontol A Biol Sci Med Sci 50 Spec No(1995) 5-8.

[2] S. Fulster, M. Tacke, A. Sandek, N. Ebner, C. Tschope, W. Doehner, S.D. Anker, S. von Haehling, Muscle wasting in patients with chronic heart failure: results from the studies investigating co-morbidities aggravating heart failure (SICA-HF), Eur Heart J 34(7) (2013) 512-519.

[3] R.H. Mak, A.T. Ikizler, C.P. Kovesdy, D.S. Raj, P. Stenvinkel, K. Kalantar-Zadeh, Wasting in chronic kidney disease, J Cachexia Sarcopenia Muscle 2(1) (2011) 9-25.

[4] T.N. Kim, M.S. Park, S.J. Yang, H.J. Yoo, H.J. Kang, W. Song, J.A. Seo, S.G. Kim, N.H. Kim, S.H. Baik, D.S. Choi, K.M. Choi, Prevalence and determinant factors of sarcopenia in patients with type 2 diabetes: the Korean Sarcopenic Obesity Study (KSOS), Diabetes Care 33(7) (2010) 1497-1499.

[5] S. Lim, J.H. Kim, J.W. Yoon, S.M. Kang, S.H. Choi, Y.J. Park, K.W. Kim, J.Y. Lim, K.S. Park, H.C. Jang, Sarcopenic obesity: prevalence and association with metabolic syndrome in the Korean Longitudinal Study on Health and Aging (KLoSHA), Diabetes Care 33(7) (2010) 1652-1654.

[6] G.S. Lynch, Therapies for improving muscle function in neuromuscular disorders, Exerc Sport Sci Rev 29(4) (2001) 141-148.

[7] F. Derbre, B. Ferrando, M.C. Gomez-Cabrera, F. Sanchis-Gomar, V.E. Martinez-Bello, G. Olaso-Gonzalez, A. Diaz, A. Gratas-Delamarche, M. Cerda, J. Vina, Inhibition of xanthine oxidase by allopurinol prevents skeletal muscle atrophy: role of p38 MAPKinase and E3 ubiquitin ligases, PLoS One 7(10) (2012) e46668.

[8] C. Fermoselle, R. Rabinovich, P. Ausin, E. Puig-Vilanova, C. Coronell, F. Sanchez, J. Roca, J. Gea, E. Barreiro, Does oxidative stress modulate limb muscle atrophy in severe COPD patients?, Eur Respir J 40(4) (2012) 851-862.

[9] K.S. Beetham, E.J. Howden, D.M. Small, D.R. Briskey, M. Rossi, N. Isbel, J.S. Coombes, Oxidative stress contributes to muscle atrophy in chronic kidney disease patients, Redox Rep 20(3) (2015) 126-132.

[10] E. Barreiro, J. Gea, M. Di Falco, L. Kriazhev, S. James, S.N. Hussain, Protein carbonyl formation in the diaphragm, Am J Respir Cell Mol Biol 32(1) (2005) 9-17.

[11] T.F. Cunha, A.V. Bacurau, J.B. Moreira, N.A. Paixao, J.C. Campos, J.C. Ferreira, M.L. Leal, C.E. Negrao, A.S. Moriscot, U. Wisloff, P.C. Brum, Exercise training prevents oxidative stress and ubiquitin-proteasome system overactivity and reverse skeletal muscle atrophy in heart failure, PLoS One 7(8) (2012) e41701.

[12] S.M. Phillips, E.I. Glover, M.J. Rennie, Alterations of protein turnover underlying disuse atrophy in human skeletal muscle, J Appl Physiol (1985) 107(3) (2009) 645-654.

[13] M.D. Gomes, S.H. Lecker, R.T. Jagoe, A. Navon, A.L. Goldberg, Atrogin-1, a muscle-specific F-box protein highly expressed during muscle atrophy, Proc Natl Acad Sci U S A 98(25) (2001) 14440-14445.

[14] S.C. Bodine, E. Latres, S. Baumhueter, V.K. Lai, L. Nunez, B.A. Clarke, W.T. Poueymirou, F.J. Panaro, E. Na, K. Dharmarajan, Z.Q. Pan, D.M. Valenzuela, T.M. DeChiara, T.N. Stitt, G.D. Yancopoulos, D.J. Glass, Identification of ubiquitin ligases required for skeletal muscle atrophy, Science 294(5547) (2001) 1704-1708.

[15] N.C. Andrews, Disorders of iron metabolism, N Engl J Med 341(26) (1999) 1986-1995.

[16] G. Cairo, S. Recalcati, A. Pietrangelo, G. Minotti, The iron regulatory proteins: targets and modulators of free radical reactions and oxidative damage, Free Radic Biol Med 32(12) (2002) 1237-1243.

[17] M. Nakano, Y. Kawanishi, S. Kamohara, Y. Uchida, M. Shiota, Y. Inatomi, T. Komori, K. Miyazawa, K. Gondo, I. Yamasawa, Oxidative DNA damage (8-hydroxydeoxyguanosine) and body iron status: a study on 2507 healthy people, Free Radic Biol Med 35(7) (2003) 826-832.

[18] C. Camaschella, Understanding iron homeostasis through genetic

analysis of hemochromatosis and related disorders, Blood 106(12) (2005) 3710-3717.

[19] H. Hayashi, T. Takikawa, N. Nishimura, M. Yano, Serum aminotransferase levels as an indicator of the effectiveness of venesection for chronic hepatitis C, J Hepatol 22(3) (1995) 268-271.

[20] T. Iwasaki, A. Nakajima, M. Yoneda, Y. Yamada, K. Mukasa, K. Fujita, N. Fujisawa, K. Wada, Y. Terauchi, Serum ferritin is associated with visceral fat area and subcutaneous fat area, Diabetes Care 28(10) (2005) 2486-2491.

[21] E.S. Ford, M.E. Cogswell, Diabetes and serum ferritin concentration among U.S. adults, Diabetes Care 22(12) (1999) 1978-1983.

[22] D.H. Lee, D.Y. Liu, D.R. Jacobs, Jr., H.R. Shin, K. Song, I.K. Lee, B. Kim, R.C. Hider, Common presence of non-transferrin-bound iron among patients with type 2 diabetes, Diabetes Care 29(5) (2006) 1090-1095.

[23] J.T. Salonen, K. Nyyssonen, H. Korpela, J. Tuomilehto, R. Seppanen, R. Salonen, High stored iron levels are associated with excess risk of myocardial infarction in eastern Finnish men, Circulation 86(3) (1992) 803-811.

[24] A. Menke, J.M. Fernandez-Real, P. Muntner, E. Guallar, The association of biomarkers of iron status with peripheral arterial disease in US adults, BMC Cardiovasc Disord 9(2009) 34.

[25] T. Nakanishi, T. Kuragano, M. Nanami, Y. Otaki, H. Nonoguchi, Y. Hasuike, Importance of ferritin for optimizing anemia therapy in chronic kidney disease, Am J Nephrol 32(5) (2010) 439-446.

[26] H. Hayashi, T. Takikawa, N. Nishimura, M. Yano, T. Isomura, N. Sakamoto, Improvement of serum aminotransferase levels after phlebotomy in patients with chronic active hepatitis C and excess hepatic iron, Am J Gastroenterol 89(7) (1994) 986-988.

[27] M.P. Cuajungco, K.Y. Faget, X. Huang, R.E. Tanzi, A.I. Bush, Metal chelation as a potential therapy for Alzheimer's disease, Ann N Y Acad Sci 920(2000) 292-304.

[28] P. Cutler, Deferoxamine therapy in high-ferritin diabetes, Diabetes 38(10) (1989) 1207-1210.

[29] S. Tajima, Y. Ikeda, K. Sawada, N. Yamano, Y. Horinouchi, Y. Kihira, K. Ishizawa, Y. Izawa-Ishizawa, K. Kawazoe, S. Tomita, K. Minakuchi, K. Tsuchiya, T. Tamaki, Iron reduction by deferoxamine leads to amelioration of adiposity via the regulation of oxidative stress and inflammation in obese and type 2 diabetes KKAy mice, Am J Physiol Endocrinol Metab 302(1) (2012) E77-86.

[30] Y. Naito, S. Hirotani, H. Sawada, H. Akahori, T. Tsujino, T. Masuyama, Dietary iron restriction prevents hypertensive cardiovascular remodeling in dahl salt-sensitive rats, Hypertension 57(3) (2011) 497-504.

[31] N. Ishizaka, K. Saito, I. Mori, G. Matsuzaki, M. Ohno, R. Nagai, Iron chelation suppresses ferritin upregulation and attenuates vascular dysfunction in the aorta of angiotensin II-infused rats, Arterioscler Thromb Vasc Biol 25(11) (2005) 2282-2288.

[32] Y. Ikeda, H. Enomoto, S. Tajima, Y. Izawa-Ishizawa, Y. Kihira, K. Ishizawa, S. Tomita, K. Tsuchiya, T. Tamaki, Dietary iron restriction inhibits progression of diabetic nephropathy in db/db mice, Am J Physiol Renal Physiol 304(7) (2013) F1028-1036.

[33] M. Altun, E. Edstrom, E. Spooner, A. Flores-Moralez, E. Bergman, P. Tollet-Egnell, G. Norstedt, B.M. Kessler, B. Ulfhake, Iron load and redox stress in skeletal muscle of aged rats, Muscle Nerve 36(2) (2007) 223-233.

[34] K.C. DeRuisseau, Y.M. Park, L.R. DeRuisseau, P.M. Cowley, C.H. Fazen, R.P. Doyle, Aging-related changes in the iron status of skeletal muscle, Exp Gerontol 48(11) (2013) 1294-1302.

[35] J. Xu, M.D. Knutson, C.S. Carter, C. Leeuwenburgh, Iron accumulation with age, oxidative stress and functional decline, PLoS One 3(8) (2008) e2865.

[36] J. Xu, J.C. Hwang, H.A. Lees, S.E. Wohlgemuth, M.D. Knutson, A.R. Judge, E.E. Dupont-Versteegden, E. Marzetti, C. Leeuwenburgh, Long-term perturbation of muscle iron homeostasis following hindlimb suspension in old rats is associated with high levels of oxidative stress and impaired recovery from atrophy, Exp Gerontol

47(1) (2012) 100-108.
[37] J.Y. Chung, H.T. Kang, D.C. Lee, H.R. Lee, Y.J. Lee, Body composition and its association with cardiometabolic risk factors in the elderly: a focus on sarcopenic obesity, Arch Gerontol Geriatr 56(1) (2013) 270-278.
[38] T.H. Kim, H.J. Hwang, S.H. Kim, Relationship between serum ferritin levels and sarcopenia in Korean females aged 60 years and older using the fourth Korea National Health and Nutrition Examination Survey (KNHANES IV-2, 3), 2008-2009, PLoS One 9(2) (2014) e90105.
[39] T.F. Reardon, D.G. Allen, Iron injections in mice increase skeletal muscle iron content, induce oxidative stress and reduce exercise performance, Exp Physiol 94(6) (2009) 720-730.
[40] Y. Ikeda, S. Tajima, Y. Izawa-Ishizawa, Y. Kihira, K. Ishizawa, S. Tomita, K. Tsuchiya, T. Tamaki, Estrogen regulates hepcidin expression via GPR30-BMP6-dependent signaling in hepatocytes, PLoS One 7(7) (2012) e40465.
[41] T.N. Stitt, D. Drujan, B.A. Clarke, F. Panaro, Y. Timofeyva, W.O. Kline, M. Gonzalez, G.D. Yancopoulos, D.J. Glass, The IGF-1/PI3K/Akt pathway prevents expression of muscle atrophy-induced ubiquitin ligases by inhibiting FOXO transcription factors, Mol Cell 14(3) (2004) 395-403.
[42] M.A. Ruegg, D.J. Glass, Molecular mechanisms and treatment options for muscle wasting diseases, Annu Rev Pharmacol Toxicol 51(2011) 373-395.
[43] R.D. Klausner, J.B. Harford, cis-trans models for post-transcriptional gene regulation, Science 246(4932) (1989) 870-872.
[44] A. Jacobs, M. Worwood, Ferritin in serum. Clinical and biochemical implications, N Engl J Med 292(18) (1975) 951-956.
[45] L.L. Miller, S.C. Miller, S.V. Torti, Y. Tsuji, F.M. Torti, Iron-independent induction of ferritin H chain by tumor necrosis factor, Proc Natl Acad Sci U S A 88(11) (1991) 4946-4950.
[46] J.T. Rogers, Ferritin translation by interleukin-1and interleukin-6: the role of sequences upstream of the start codons of the heavy and light

subunit genes, Blood 87(6) (1996) 2525-2537.
[47] G.S. Hotamisligil, Inflammation and metabolic disorders, Nature 444(7121) (2006) 860-867.
[48] C.N. Lumeng, A.R. Saltiel, Inflammatory links between obesity and metabolic disease, J Clin Invest 121(6) (2011) 2111-2117.
[49] T. Hofer, E. Marzetti, J. Xu, A.Y. Seo, S. Gulec, M.D. Knutson, C. Leeuwenburgh, E.E. Dupont-Versteegden, Increased iron content and RNA oxidative damage in skeletal muscle with aging and disuse atrophy, Exp Gerontol 43(6) (2008) 563-570.
[50] H. Kondo, M. Miura, J. Kodama, S.M. Ahmed, Y. Itokawa, Role of iron in oxidative stress in skeletal muscle atrophied by immobilization, Pflugers Arch 421(2-3) (1992) 295-297.
[51] A.L. Goldberg, Protein turnover in skeletal muscle. II. Effects of denervation and cortisone on protein catabolism in skeletal muscle, J Biol Chem 244(12) (1969) 3223-3229.
[52] M.B. Metzger, V.A. Hristova, A.M. Weissman, HECT and RING finger families of E3 ubiquitin ligases at a glance, J Cell Sci 125(Pt 3) (2012) 531-537.
[53] S.H. Lecker, R.T. Jagoe, A. Gilbert, M. Gomes, V. Baracos, J. Bailey, S.R. Price, W.E. Mitch, A.L. Goldberg, Multiple types of skeletal muscle atrophy involve a common program of changes in gene expression, FASEB J 18(1) (2004) 39-51.
[54] A.M. Hanson, B.C. Harrison, M.H. Young, L.S. Stodieck, V.L. Ferguson, Longitudinal characterization of functional, morphologic, and biochemical adaptations in mouse skeletal muscle with hindlimb suspension, Muscle Nerve 48(3) (2013) 393-402.
[55] M. Sandri, C. Sandri, A. Gilbert, C. Skurk, E. Calabria, A. Picard, K. Walsh, S. Schiaffino, S.H. Lecker, A.L. Goldberg, Foxo transcription factors induce the atrophy-related ubiquitin ligase atrogin-1 and cause skeletal muscle atrophy, Cell 117(3) (2004) 399-412.
[56] C. Mammucari, G. Milan, V. Romanello, E. Masiero, R. Rudolf, P. Del Piccolo, S.J. Burden, R. Di Lisi, C. Sandri, J. Zhao, A.L. Goldberg, S. Schiaffino, M. Sandri, FoxO3 controls autophagy in skeletal muscle in

vivo, Cell Metab 6(6) (2007) 458-471.
[57] J. Zhao, J.J. Brault, A. Schild, P. Cao, M. Sandri, S. Schiaffino, S.H. Lecker, A.L. Goldberg, FoxO3 coordinately activates protein degradation by the autophagic/lysosomal and proteasomal pathways in atrophying muscle cells, Cell Metab 6(6) (2007) 472-483.
[58] T.J. McLoughlin, S.M. Smith, A.D. DeLong, H. Wang, T.G. Unterman, K.A. Esser, FoxO1 induces apoptosis in skeletal myotubes in a DNA-binding-dependent manner, Am J Physiol Cell Physiol 297(3) (2009) C548-555.
[59] Y. Kamei, S. Miura, M. Suzuki, Y. Kai, J. Mizukami, T. Taniguchi, K. Mochida, T. Hata, J. Matsuda, H. Aburatani, I. Nishino, O. Ezaki, Skeletal muscle FOXO1 (FKHR) transgenic mice have less skeletal muscle mass, down-regulated Type I (slow twitch/red muscle) fiber genes, and impaired glycemic control, J Biol Chem 279(39) (2004) 41114-41123.
[60] Y. Wang, M. Wu, R. Al-Rousan, H. Liu, J. Fannin, S. Paturi, R.K. Arvapalli, A. Katta, S.K. Kakarla, K.M. Rice, W.E. Triest, E.R. Blough, Iron-induced cardiac damage: role of apoptosis and deferasirox intervention, J Pharmacol Exp Ther 336(1) (2011) 56-63.

Table

Table.1 Characteristics of Body weight and skeletal muscles weight

	Pre		Day 7		Day 14	
	Vehicle	Fe	Vehicle	Fe	Vehicle	Fe
Body weight (g)	22.4 ± 0.2	22.7 ± 0.2	23.3 ± 0.4	24.0 ± 0.4	23.6 ± 0.2	24.1 ± 0.3
Gastrocunemius muscle (mg)	—	—	139.8 ± 3.0	125.1 ± 2.8**	135.9 ± 3.8	122.5 ± 1.8**
Soleus muscle (mg)	—	—	8.2 ± 0.2	6.3 ± 0.3**	8.3 ± 0.3	7.0 ± 0.2**
Tibialis anterior muscle (mg)	—	—	70.6 ± 1.9	64.8 ± 1.5*	68.9 ± 3.6	58.1 ± 2.1*

Data are the mean ± SEM, n = 10–18, as indicated. *P < 0.05, **P < 0.01 vs. vehicle treatment at the same time

Table.2 Changes of skeletal muscle iron content serum ferritin concentration

	Vehicle	Fe day 1	Fe day 3	Fe day 7	Fe day 14
Gastrocunemius muscle iron (μg / g muscle weight)	10.1 ± 0.3	12.3 ± 0.9	17.5 ± 0.6*	20.4 ± 0.7*	23.7 ± 1.3**
Serum ferritin (ng/ml)	490 ± 20	1481 ± 987	9690 ± 2127**	33892 ± 1106**	46405 ± 6292**

Data are the mean ± SEM, n = 6–12, as indicated. *P < 0.05, **P < 0.01 vs. vehicle treatment

Figure

Figure 1 Ikeda, et al.

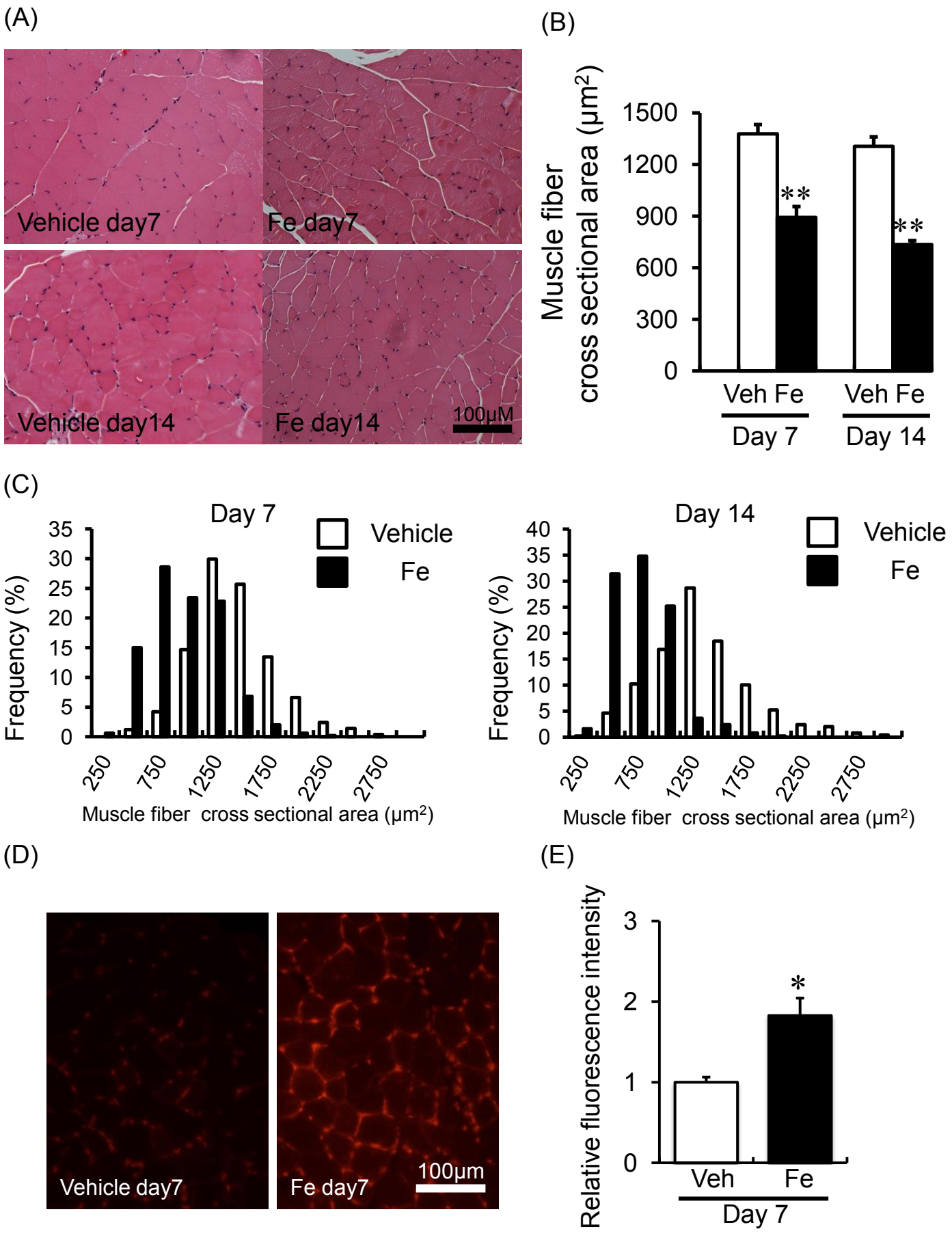

Figure 1 continued

(F)

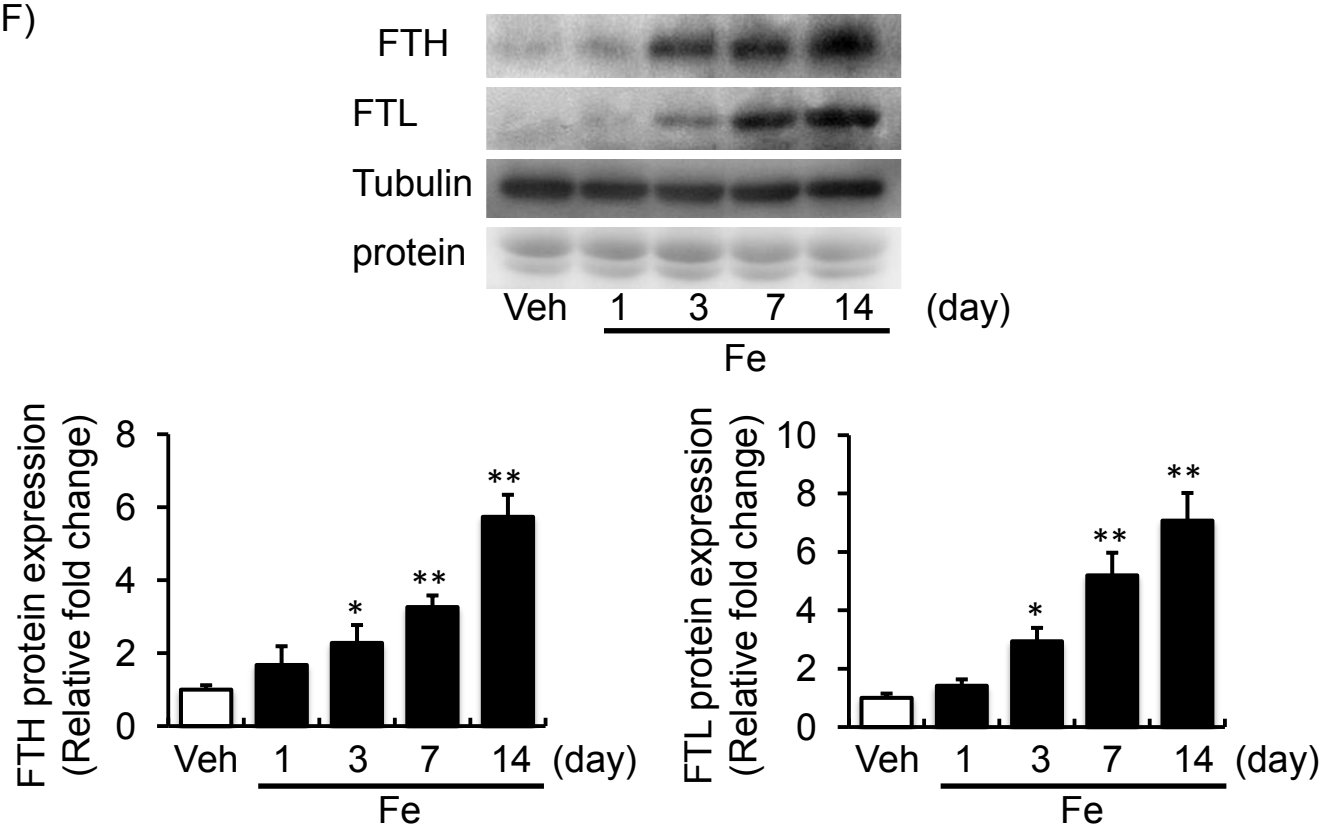

Figure 2 Ikeda, et al.

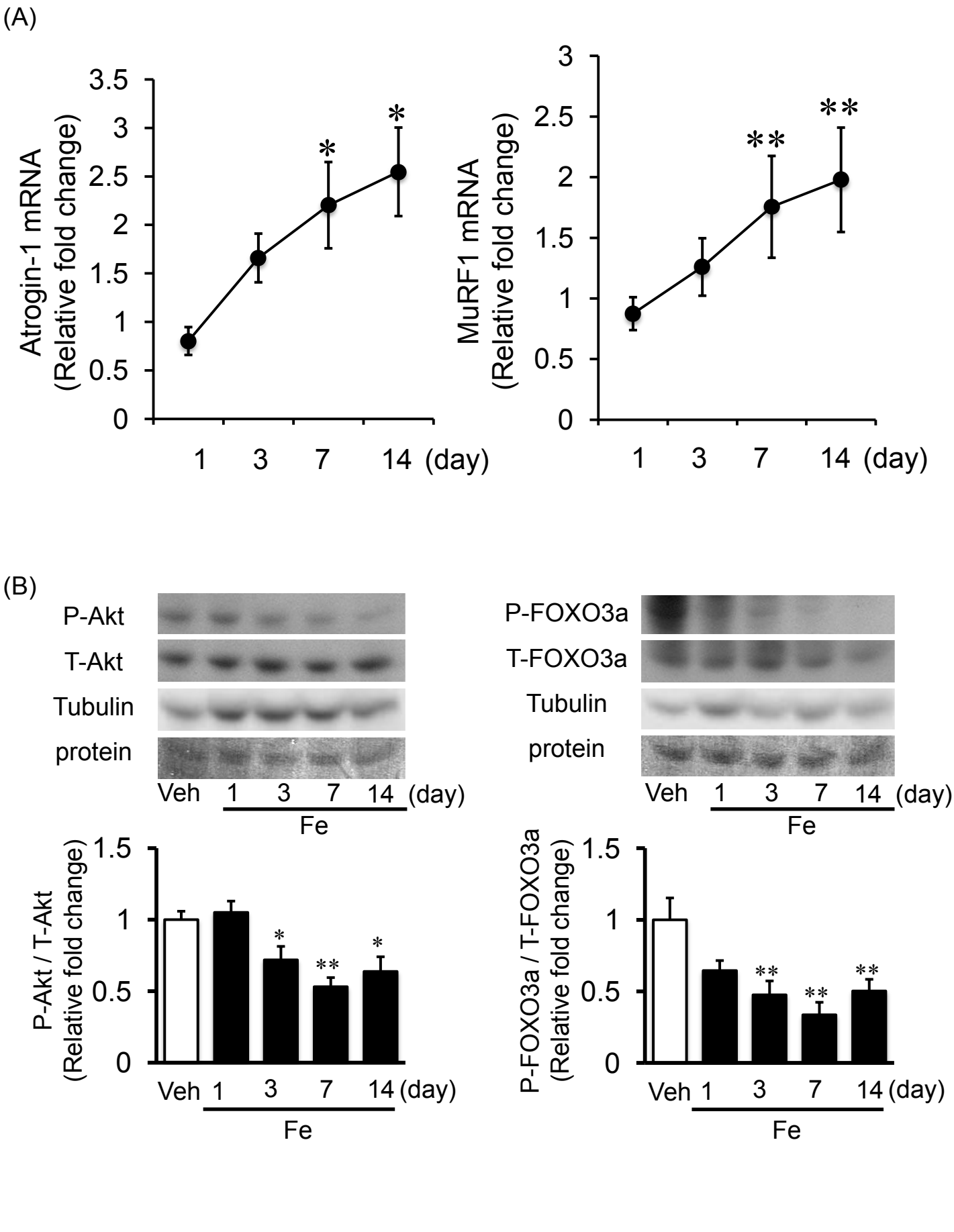

Figure 3 Ikeda, et al.

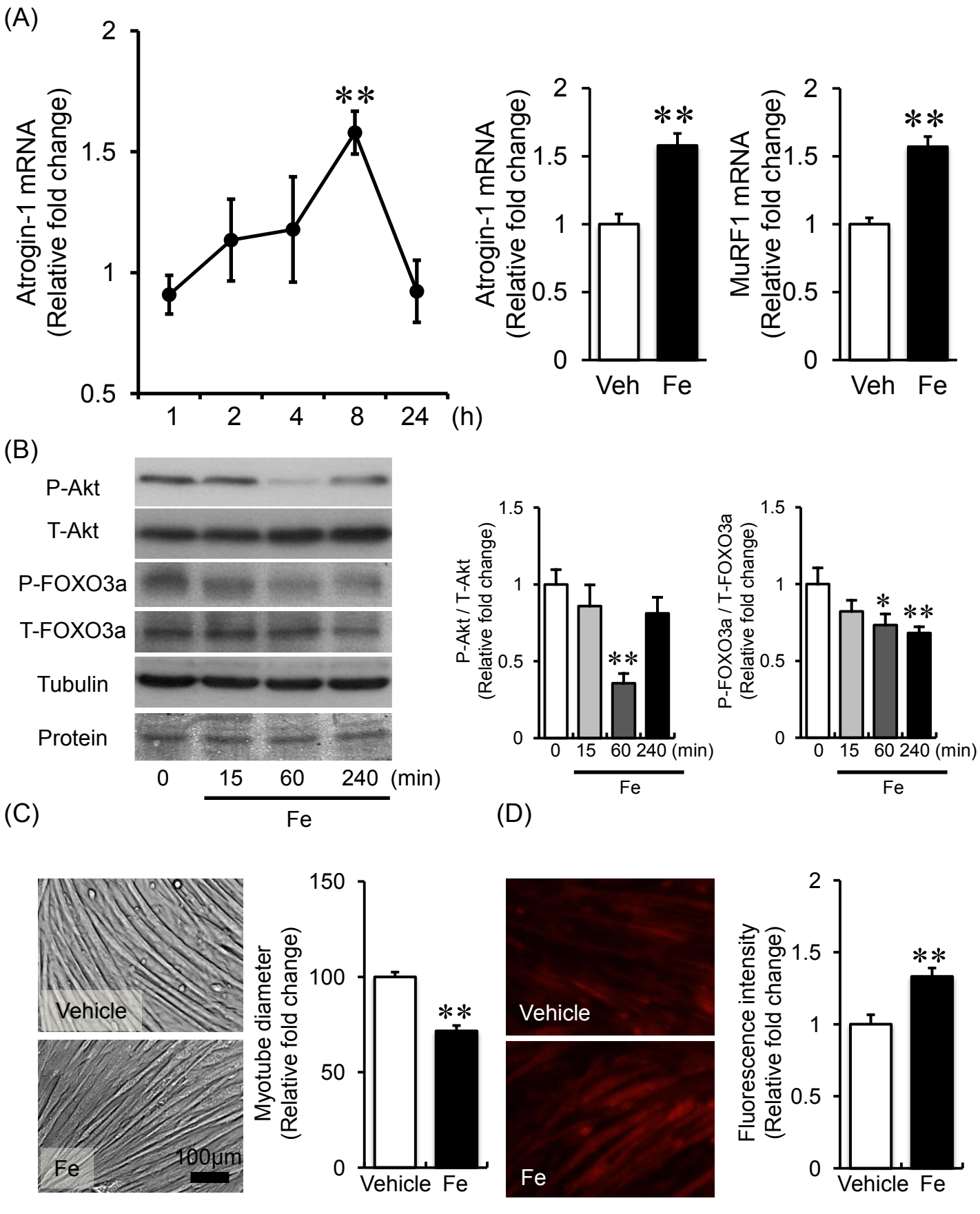

Figure 4 Ikeda, et al.

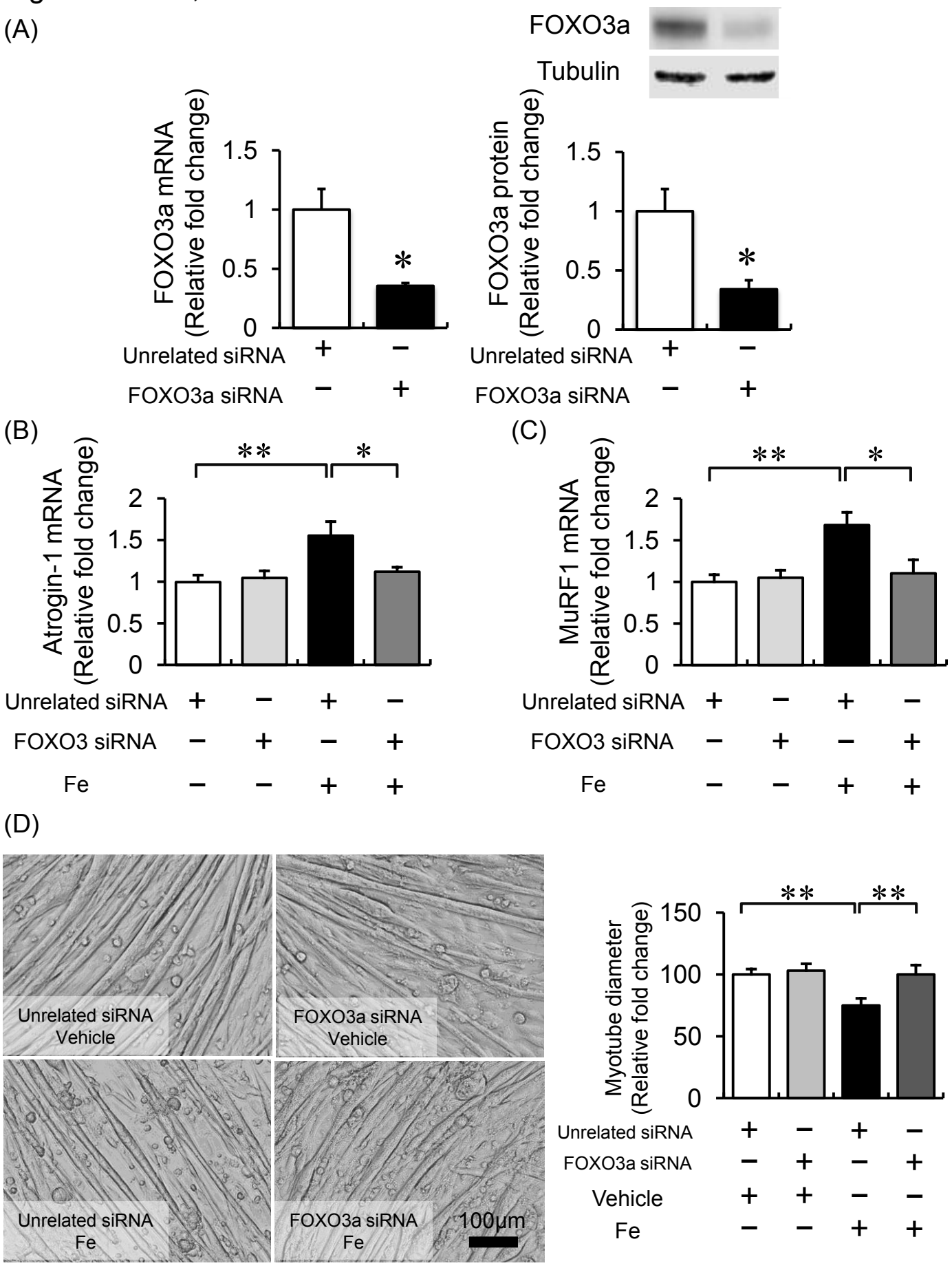

Figure 5 Ikeda, et al.